The effects of distributed electric propulsion on the aerodynamics of a regional aircraft wing

Dennis Stefan CHELEMEN*,[1], Ionut BUNESCU*,[1,2], Mihai-Victor PRICOP[2], Mihaita-Gilbert STOICAN[2]

*Corresponding author
[1]Department of Aerospace Sciences, POLITEHNICA University Bucharest, Splaiul Independentei 313, 060042, Bucharest, Romania, dennis.chelemen@stud.aero.upb.ro*
[2]INCAS – National Institute for Aerospace Research "Elie Carafoli", B-dul Iuliu Maniu 220, Bucharest 061126, Romania, bunescu.ionut@incas.ro*, pricop.victor@incas.ro, stoican.gilbert@incas.ro

DOI: 10.13111/2066-8201.2023.15.4.6

Received: 29 September 2023/ Accepted: 06 November 2023/ Published: December 2023

Abstract: *A study is performed to comprehensively evaluate the aerodynamic performance of a regional aircraft designed for short-haul flights, with a particular focus on the effects of distributed electric propulsion (DEP) on aerodynamic performances. This effort aligns well with a core objective of the Clean Aviation program to decrease carbon emissions within the aviation sector. To address this challenge, we propose a concept that considers incorporating electric motors to complement the conventional propulsion system of a regional aircraft wing. These electric motors have the capability to draw power from either the traditional turboprop engine or exclusively from an on-board electrical generator, providing an innovative pathway for emissions reduction. The central focus of this study revolves around a detailed examination of the aerodynamic efficacy with respect to the placement of engines within the wing. It seeks to ascertain whether optimal aerodynamic efficiency is achieved through the adoption of a greater number of smaller-diameter motors, characterized by reduced power output to the shaft. Alternatively, the study explores the prospect of employing a reduced number of motors, each possessing larger diameters and correspondingly augmented power output. While a larger motor size may intuitively suggest superiority in terms of thrust, it remains imperative to meticulously evaluate the potential influence of the associated drag factor. This research contributes to the growing body of knowledge in the realm of aviation by shedding light on the intricate interaction between aerodynamic efficiency and power output in the context of propulsion system design.*

Key Words: *Panel Method, Distributed Electric Propulsion, Hybrid Serial/Parallel Propulsion, Propulsion Positioning Effects, Regional Aircraft*

1. INTRODUCTION

The objective of this study is to assess the aerodynamic efficiency of various engine configurations, particularly to ascertain whether optimal performance is achieved by employing multiple smaller motors with reduced power or fewer larger motors with greater power. While larger motors may seem better, it is important to consider the impact of drag. This paper continues the previous research on the effects of distributed electric propulsion in aerodynamic performances [1], [2], [3], [4], [5], [6], stability and control [7], [8], and energy

consumption [9]. As in previous studies [2], [7], [8], [9], in the current research a wing model for a regional aircraft in both hybrid-electric and full-electric configurations has been considered. This study aims to improve the aerodynamic performance and reduce the energy consumption by using electric motors and implementing distributed electric propulsion (DEP). The objectives of this work are in line with the Clean Aviation program initiatives to reduce emissions by studying the feasibility of implementing disruptive aviation technologies. Various research scenarios involving different power levels (25%, 50%, 75% and 100%), nacelle positions (middle, upper and lower), spin direction (clockwise or counter clockwise) and number of propellers (one-to-four) will be examined using four different cases, as illustrated below.

Table 1 – Considered cases

Name	25p 1	25p 2	25p 3	25p 4	50p 1	50p 2	50p 3	50p 4	75p 1	75p 2	75p 3	75p 4	100 p1	100 p2	100 p3	100p 4
Power	25%				50%				75%				100%			
Prop.	1	2	3	4	1	2	3	4	1	2	3	4	1	2	3	4
Spin Dir.	Cw/ Ccw	Ccw	Ccw	Cw/ Ccw	Cw/ Ccw	Ccw	Ccw	Cw/ Ccw	Cw/ Ccw	Ccw	Ccw	Cw/ Ccw	Ccw	Ccw	Ccw	Ccw
Z pos.	M	M	M	L, M, U	M	M	M	M	M	M	M	L, M, U	M	M	M	M

Table 1 shows the cases to be analyzed. The power ratio (*Power*) represents the fraction of total power used by the electric motors. The sub-unitary fractions represent the hybrid-electric cases, and the unitary power ratio represents the full-electric cases. The hybrid-electric configuration consists of a turboprop engine and electric motors, with the former providing power to the latter. For the full-electric cases, a clean wing with electric motors only have been adopted. The number of propellers (*Prop.*) indicates to the count of electric motors considered in the study while, the spin direction (*Spin Dir.*) denotes the rotational orientation of the propeller blades which can either be clockwise (*Cw*) or counter clockwise (*Ccw*). The Z position (*Z pos.*) signifies propellers position relative to the wing plane, which can be in the wing plane (*M*), above it (*U*), or below it(*L*). In order to established a comparative reference, two additional scenarios were examined: one involving a wing with a turboprop engine (pertaining to the hybrid-electric configuration), and the other featuring, a clean wing (representing the full-electric configuration). The turboprop engine presents a propeller diameter equal to *4m* and an angular velocity equal to *1200rpm*. The electric motors present propellers with different diameters between 1.3m (four motors) and 2m (one motor) and a constant angular velocity equal to *3000rpm*. To find a consistent pattern among the electric motors already in use in aviation, a regression line was obtained between the nacelle's diameter and the motor power. This regression line is shown in Fig. 1:

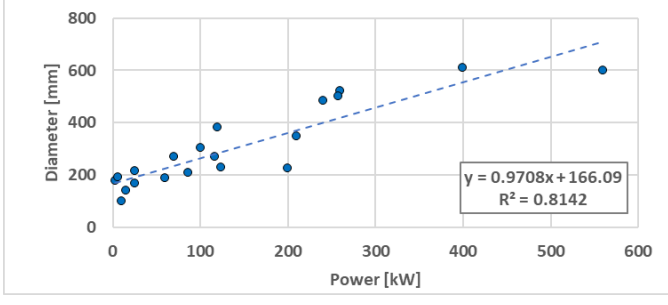

Fig. 1 – Nacelle's diameter as function of motor's power

Thus, the nacelle diameters can be calculated using the linear equation above, which is a function of the motor power. The motor power will vary from study case to study case.

The study hypothesis considers a uniform flight with constant velocity *V=150m/s* at angle of attack $\alpha = 2°$ and altitude equal to *6000m* (p=47181Pa, ρ= 0.6597kg/m^3, *T=249.15K*, *a=316.428m/s*, μ=1.61^{-5} *Pa s*). The power developed by one turboprop engine is *1500kW* resulting in a thrust force equal to *10kN*. This force is used as a total force developed by the turboprop engine and electric motors.

2. MATHEMATICAL MODELING

2.1 Geometry description

The considered geometries consist in a regional aircraft wing (MAC = 2.25m, S_{ref} = 61m^2) which equip a turboprop engine and one or more electric motors. Table 1 defines all analyzed cases presenting the number of motors considered. The geometries used in this study were designed to isolate the wing and nacelles from the fuselage, so that only the wing-propeller interaction could be studied in a focused way. The electrical motor positions along the wingspan are presented in Table 2:

Table 2 – Positions of motors for each case

Configuration		0 (Turbo-prop)	1 (Electric)	2 (Electric)	3 (Electric)	4 (Electric)
Hybrid-electric	Baseline	y = 3.3 m	None	None	None	None
	Case 1	y = 3.3 m	y = 11.5 m	None	None	None
	Case 2	y = 3.3 m	y = 11.5 m	y = 6.9 m	None	None
	Case 3	y = 3.3 m	y = 11.5 m	y = 9.4 m	y = 7.3 m	None
	Case 4	y = 3.3 m	y = 11.5 m	y = 9.9 m	y = 8.3 m	y = 6.8 m
Full-electric	Baseline	None	None	None	None	None
	Case 1	None	y = 11.5 m	None	None	None
	Case 2	None	y = 11.5 m	y = 8.6 m	None	None
	Case 3	None	y = 11.5 m	y = 8.6 m	y = 5.7 m	None
	Case 4	None	y = 11.5 m	y = 8.6 m	y = 5.7 m	y = 2.8 m

This paper analyzes 10 aircraft geometries with different propeller spin directions, powers, and locations on the z-axis. Two examples of these geometries are shown below.

In Fig. 2 it can be observed the hybrid-electric configuration featuring four electric motors operating at 75% power alongside one turboprop engine.

The turboprop engine is consistently employed in all hybrid-electric scenarios to supply power to the electric motors, which can be operated at different power levels. Notably, the electric motors have a smaller diameter than the turboprop engine, resulting in a reduced size of the nacelles and propellers.

The hybrid-electric case has four different configurations, each with a different number of electric motors. All the electric motors in each configuration shares the same diameter, angular velocity, and thrust coefficient.

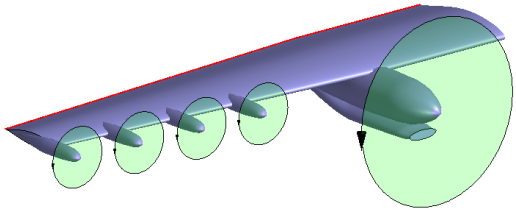

Fig. 2 – Hybrid-electric configuration (75p4 case)

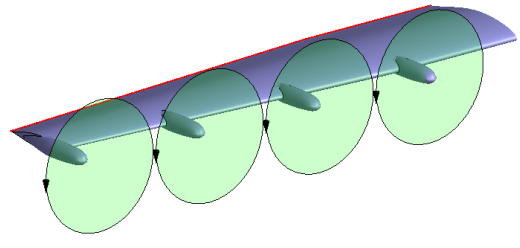

Fig. 3 – Full-electric configuration (100p4 case)

Fig. 3 shows a full-electric configuration with four electric motors with 100% power. The electric motors are powered by a source of energy inside the aircraft fuselage, which can be batteries, fuel cells, or a turbo-shaft engine.

The full-electric case also has four configurations with different numbers of motors. The motors and propellers have identical characteristics (thrust coefficient, diameter, and angular velocity) to ensure a limited range of analyses.

The electric motor nacelles maintain a constant distance of 900mm between their nose tip and the leading edge of the wing.

2.2 Mesh generation

To simplify the mesh generation process, the wing and nacelles were created as independent bodies. The surface meshes were created structured setting the number of panels on generators and their distribution.

This allows for high-density regions, such as the leading edge, and low-density regions, such as the middle area of the upper surface.

After establishing the independent bodies, each case was imported to performs a Boolean intersection, resulting in a unified entity. This entity represents a continuous surface with distinct sub-surfaces attributed to each of the initial bodies, facilitating the monitoring of aerodynamic loads on each body. Presented below are two examples of mesh generation illustrating the panel areas. Fig. 4 presents the mesh on the hybrid-electric configuration with four electric motors (75p4 case).

It can be observed that the area of panels varies between 0.005m^2 to 0.04m^2. The small panels are situated along the leading edge, near the nacelle nose and in the proximity to the trailing edge, , while the larger panels are positioned in the middle region of both the upper and lower surface. This mesh comprises a total 10198 panels across the entire geometry.

Fig. 5 displays the mesh of the full-electric configuration with four electric motors (100p4 case). The panels areas exhibit a similar range to the previous case, spanning from 0.005m^2 to 0.04m^2. This mesh presents 6956 panels for the entire geometry.

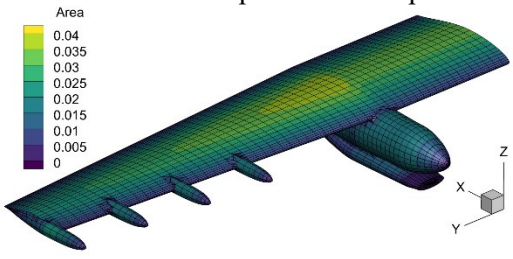

Fig. 4 – Mesh on hybrid-electric configuration

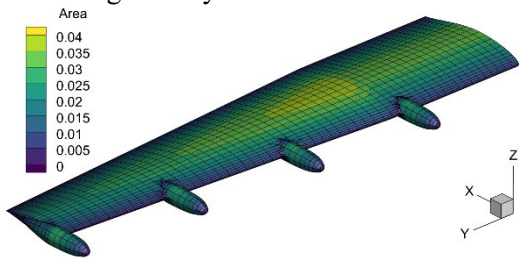

Fig. 5 – Mesh on full-electric configuration

2.3 Solver Methodology

This study employs a potential flow model with a panel method and disk actuator method to assess aerodynamics and propeller effects, offering a resource-efficient and decent accuracy, as demonstrated in [3] and [6].

At its most basic level, the method used in this study can be thought of as applying a vortex ring to the edges of a panel. This simplification helps us get a clear idea of how the system works. By using the Biot-Savart law, we can determine the speed induced by the vortex ring within a standard flat panel as it is demonstrated in [10].

This approach forms the foundation for a better understanding of the complex aerodynamic and propeller interactions that is being researched, by meshing more surfaces

along the actual surface. It entails the augmentation of panels along the actual surface and the creation of more complex shapes to closely approximate the characteristics of shape and flow.

Fig. 6 illustrates the effects that a ring vortex has on a point (P), situated at a certain horizontal and vertical distance, forming an angle between point 1 and point 2 of the facet from segment l.

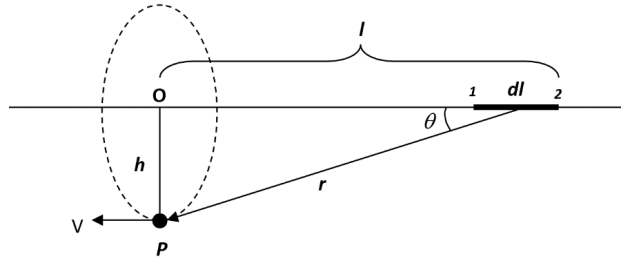

Fig. 6 – The velocity induced at a point by a segment of a facet-bound vortex ring

In accordance with the Biot-Savart Law, the deduction of induced speed begins with:

$$\mathrm{d}V_i = \frac{\Gamma \cdot \mathrm{d}l \times r}{4 \cdot \pi \cdot r^3} \tag{1}$$

After a sequence of mathematical manipulations and analytical procedures, it produces the following relation:

$$\mathrm{d}V_i = \frac{\Gamma \cdot \sin(\theta) \cdot \mathrm{d}l(\theta)}{4 \cdot \pi \cdot h} \tag{2}$$

After further integration along the whole segment:

$$V_i = \frac{\Gamma \cdot (\cos(\theta_2) - \cos(\theta_1)}{4 \cdot \pi \cdot h} \tag{3}$$

The cumulative velocity resulting from the entire plane is as follows:

$$V = \sum_{i=1}^{Nedges} V_i \tag{4}$$

The variable of interest in this equation is the circulation (Γ). The velocity at another point, denoted as '*j*,' can be formulated as:

$$V_j = \Gamma_j \sum_{i=1}^{Nedges} \frac{(\cos(\theta_{2i}) - \cos(\theta_{1i})}{4 \cdot \pi \cdot h_i} \tag{5}$$

In this context, the latter term following the circulation is considered as the geometric influence of the panel, noted with $A_{j,P}$:

$$V_j = \Gamma_j \cdot A_{j,P} \tag{6}$$

This can be represented as a matrix in the following manner:

$$\begin{bmatrix} A_{1,1} & \cdots & A_{1,N} \\ \vdots & \ddots & \vdots \\ A_{N,1} & \cdots & A_{N,N} \end{bmatrix} \begin{bmatrix} \Gamma_1 \\ \cdots \\ \Gamma_N \end{bmatrix} = \begin{bmatrix} \mathrm{B}_i \\ \cdots \\ \mathrm{B}_N \end{bmatrix} \tag{7}$$

In this context, the matrix 'B' represents the initial velocity condition. Through the application of matrix inversion, it is possible to ascertain the circulation array component, a key variable enabling the determination of the aerodynamic load distribution along the wing. Furthermore, this process allows for the determination of additional aerodynamic characteristics, such as the induced drag. The calculation of lift-induced and induced drag can be achieved through the following aerodynamic relationships:

$$L_{induced} = \int_{-b}^{b} \rho_{\infty} V_{\infty} \Gamma_y dy \tag{8}$$

$$D_{induced} = \int_{-b}^{b} \rho_{\infty} w_y \Gamma_y dy \tag{9}$$

where b is the wingspan of a symmetric aircraft and w_y represents the induced downwash between the two consecutive integrated circulation loops at the span-wise location y

$$w_y = \frac{1}{4 \cdot \pi} \int_{-b}^{b} \left(\frac{1}{y - y_0} \right) \frac{-d\Gamma_{y_0}}{dy} dy_0 \tag{10}$$

2.3 Solver settings

The solver configuration involves selecting the flow parameters mentioned earlier (including a flight altitude of 6000m), choosing the trailing edge and its length, picking base regions if they are present, and configuring the settings for disk actuators (including the reference system, diameter, thrust coefficient, and angular speed).

In Fig. 7, an isometric-front view displays the simulation components. The electric motors, the wing, and the turboprop sub-surfaces are designated as having wall boundary conditions. The actuator disks are surfaces that enable the passage of flow, inducing additional speed components.

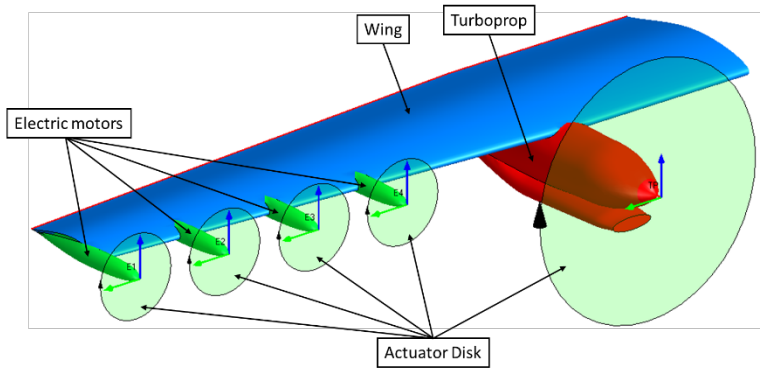

Fig. 7 – Case setting: front view

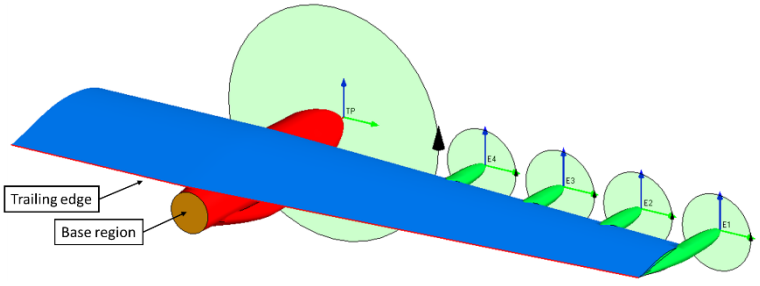

Fig. 8 – Case setting: back view

Fig. 8 illustrates the simulation components from an isometric-back view. It is important to note that in order to accurately assess the aerodynamic forces, it is essential to configure the trailing edge and the base regions, if present, as demonstrated below.

3. RESULTS AND DISCUSSIONS

3.1 Effect of positioning on Oy axis on lift coefficient

The first study is the simplest analysis of the effect of the motor's lateral position on the lift distribution along the wingspan. Fig. 9 shows the variation of the lift coefficient along the wingspan for five scenarios.

One scenario is the baseline, which is a clean wing without any motor or propeller. The other four scenarios are wings with one electric motor placed at different positions (2.87m, 5.75m, 8.26m, and 11.5m, respectively) from the symmetry plane.

The figure also shows the integrated lift coefficient on the wing semi-plane in textboxes, which indicates the overall performance.

The lift coefficient of a clean wing decreases continuously from the center to the tips. Adding a motor to the wing causes a local variation in the lift coefficient around the motor, called the propeller effect.

The propeller effect varies sinusoidally, meaning that it has a repeating wave-like pattern. Compared to the clean wing, the lift coefficient is higher inboard of the motor and lower outboard of the motor. The propeller effect is negligible at a significant distance from the motor.

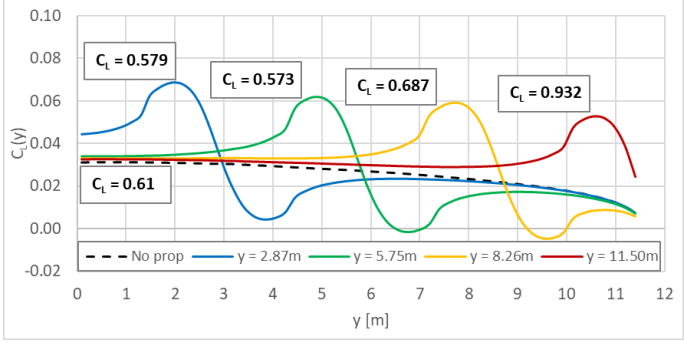

Fig. 9 – The effect of propeller lateral positioning on lift distribution along the wingspan

The integrated lift coefficient (which is the total lift generated by the wing) is highest when the motor is placed at the wingtip and spinning in the opposite direction to the tip vortex. This is because the propeller helps to reduce the strength of the tip vortex, which is a region of low pressure at the wingtip that can cause drag. The integrated lift coefficient is lowest when the motor is placed closest to the center of the wing because the propeller has less of an effect on the lift distribution in this region. At a significant distance from the motor, the lift coefficient is similar to that of a clean wing without any propellers or motors. This is because the propeller effect is only felt in the immediate vicinity of the motor.

3.2 Effect of positioning on Oz axis on lift coefficient

This study examines how the vertical placement of four electric motors affects the distribution of lift along the wingspan. Two hybrid-electric cases were considered: one with 25% power from the electric motors and one with 75% power. For each case, the motors were placed in

three different positions: in line with the wing, 0.2 meters below the wing ('L' noted), and 0.2 meters above the wing ('U' noted).

Fig. 10 shows that the vertical positioning of the propulsion system can increase or decrease the lift performance of the wing. It can be observed that the upper positioning (above the wing plane) presents higher lift coefficient values than the in-line positioning of the motors, and the lower positioning (below the wing plane) has lower lift coefficient values than the in-line positioning of the motors. That is happening because of flow velocity effect. For the upper placing the flow velocity increase generating a lower pressure on wing upper surface which increase the lift, otherwise for the lower positioning, the flow velocity increase generating also a lower pressure on wing lower surface which decrease the lift.

Both considered cases, with 25% power ratio and 75% power ratio, present similar effects, however the values are distinct due to the power effect on lift coefficient.

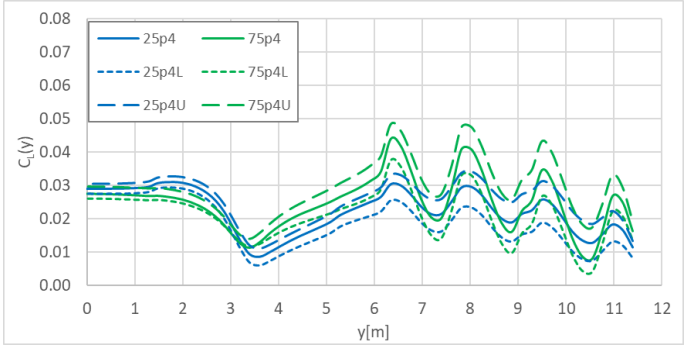

Fig. 10 – The effect of propeller vertical positioning on lift distribution along the wingspan

3.3 Effect of number of propellers on lift coefficient

This study examines the impact of propeller number on lift distribution along the wingspan of hybrid-electric and fully-electric aircraft.

The hybrid-electric configuration has three cases with varying power ratios (25%, 50%, and 75%), while the fully-electric configuration has a power ratio of 100%. Each figure below shows five curves: the baseline (wing with turboprop engine for hybrid-electric configuration and clean wing for fully-electric configuration) and four curves for the cases with one, two, three, and four electric motors. Fig. 11 a)-to-c) show the lift distribution along the wingspan of hybrid-electric aircraft with different power ratios (25%, 50% and 75%). The number of propellers affects the lift distribution, with one electric motor producing more interference than more electric motors due to the concentration of power.

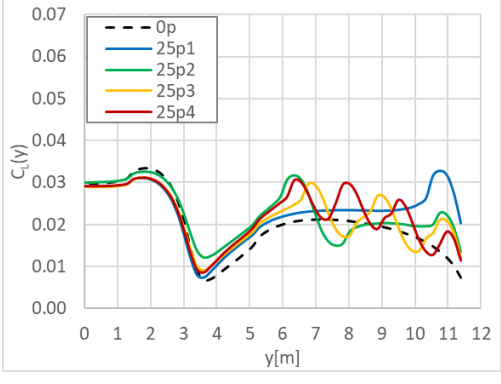

a) 25% power for electric propulsion

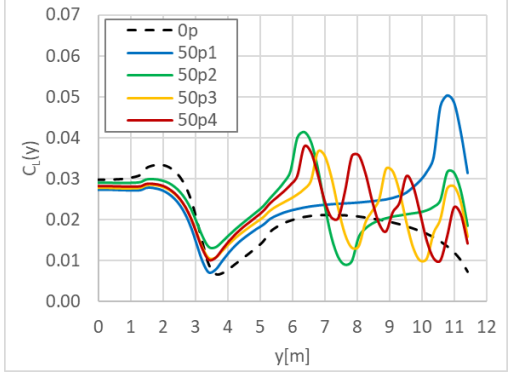

b) 50% power for electric propulsion

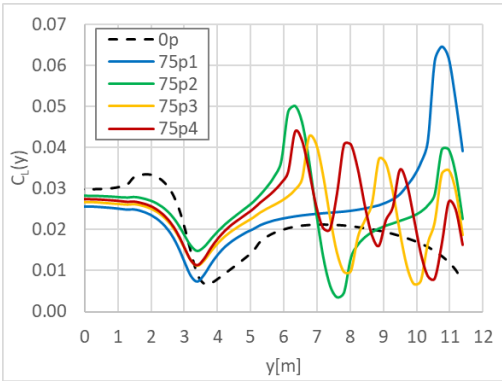

c) 75% power for electric propulsion

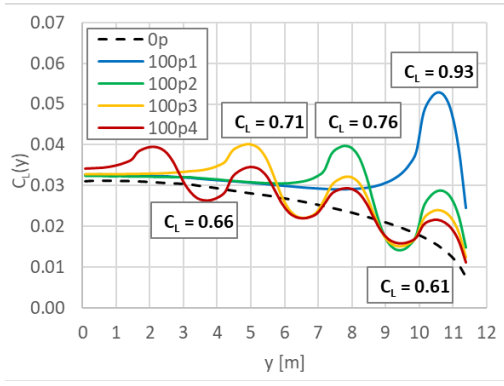

d) 100% power for electric propulsion

Fig. 11 – The effect of number of propellers on lift distribution along the wingspan

Fig. 11 d) shows the lift distribution for a full-electric aircraft with a 100% power ratio. The baseline curve shows no interference because the wing has no propellers. The cases with propellers have an electric motor on the wingtip, which significantly increases the lift coefficient. The magnitude of the interference is also highest for the case with one electric motor due to the concentration of power.

The case with a single propeller at the wingtip produces the largest increase in lift, but this case presents structural challenges due to the large tensile forces at the embedding region. All other cases show a higher total lift coefficient, demonstrating the advantages of distributed electric propulsion, such as increased lift and reduced structural tensions.

3.4 Effect of spin direction on lift coefficient

This case examines how the direction of propeller rotation affects the distribution of lift coefficient along the wingspan.

It considers two hybrid-electric cases: one propeller and four propellers at 25%, 50%, and 75% power ratios. Fig. 12 a) and b) show both clockwise (CW) and counterclockwise (CCW) propeller rotation for comparison. It is important to note that CCW propeller rotation is also the opposite direction to the rotation of the tip vortex.

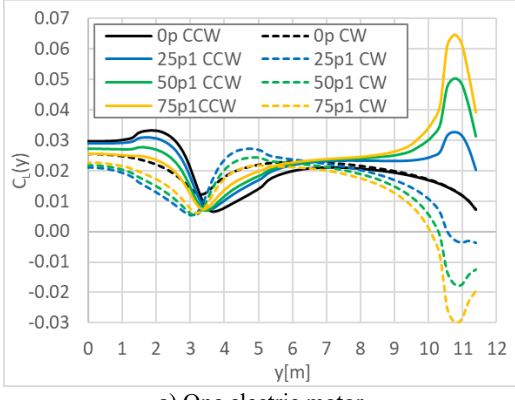

a) One electric motor

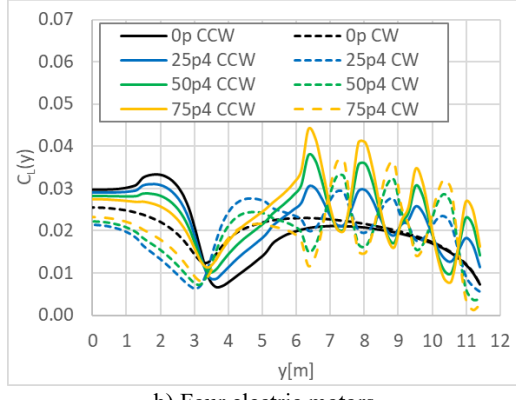

b) Four electric motors

Fig. 12 – The effect of spin direction on lift distribution along the spanwise

The first case examines how the direction of propeller rotation affects lift distribution when all the power is concentrated in one electric motor.

Figure a) shows two curves, one for clockwise (CW) rotation and one for counterclockwise (CCW) rotation.

It can be observed that the direction of propeller rotation changes the trend of the lift coefficient distribution.

When the propeller rotates counterclockwise (CCW), the lift coefficient increases on the in-board part of the wing and decreases on the out-board part of the wing. When the propeller rotates clockwise (CW), the opposite happens: the lift coefficient decreases on the in-board part of the wing and increases on the out-board part of the wing. Therefore, when the propeller is placed at the wingtip, the lift coefficient decreases significantly instead of increasing (as it does when the propeller rotates CCW).

When the propeller is placed at the wingtip and rotates clockwise (CW), the lift coefficient at the wingtip can even become negative.

This decreases the total lift coefficient of the wing. In contrast, when the propeller rotates counterclockwise (CCW), the lift at the wingtip increases significantly, increasing the total lift coefficient of the wing.

The second case examines how the direction of propeller rotation affects lift distribution when the power is distributed among four electric motors. Similar to the previous case, the figure b) shows two curves, one for clockwise (CW) rotation and one for counterclockwise (CCW) rotation. The direction of propeller rotation changes the trend of the lift coefficient distribution.

Because the electric motors have less power, the lift interference for the clockwise (CW) rotation case is smaller but still positive.

For the counterclockwise (CCW) rotation case, the lift coefficient only increases slightly for each propeller.

Therefore, the effect of propeller rotation in this case is similar to the previous case, except that the magnitude of the lift interference is smaller.

3.5 Effect of power on lift coefficient

This study examines how the number of propellers and the power of the electric motors affect the distribution of lift coefficient along the wingspan of a hybrid-electric aircraft.

The effect of the turboprop engine is included in all cases, even in the baseline case where only the turboprop engine is considered.

Fig. 13 shows that the magnitude of the interference increases with the power of the motors. Conversely, the magnitude of the interference decreases when the power is divided among more motors due to power sharing.

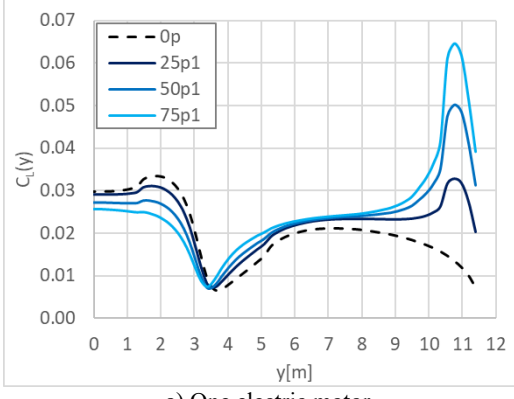

a) One electric motor

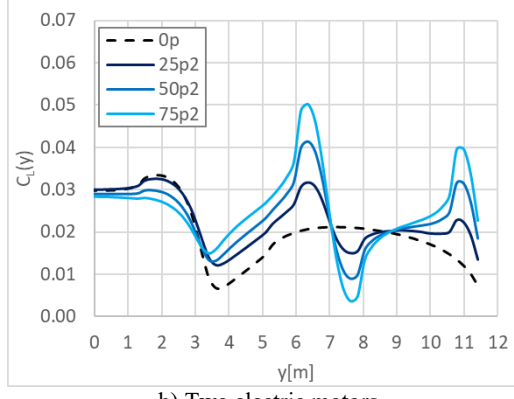

b) Two electric motors

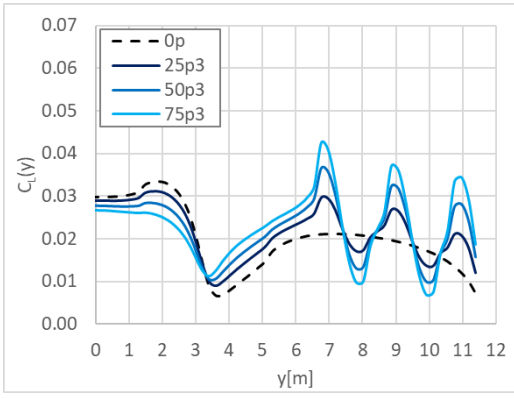

c) Three electric motors

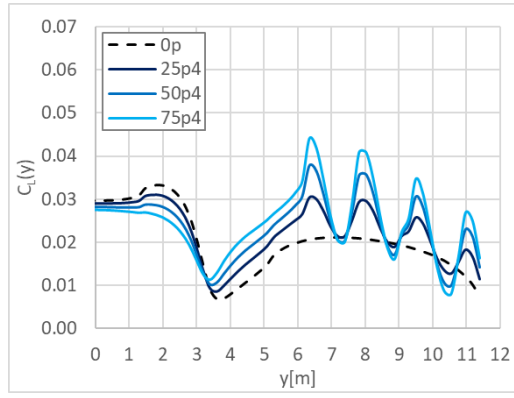

d) Four electric motors

Fig. 13 – The effect of the power of the motors on lift distribution along the wingspan

The greatest magnitude of interference occurs when there is one electric motor with 75% power. The total lift coefficient is also highest in this case because there is no negative interference at the wingtip.

3.6 Effect of configuration and number of motors on drag coefficient

Fig. 14 shows the drag coefficient for hybrid-electric and full-electric aircraft configurations with zero-to-four propellers.

The drag coefficient of the hybrid-electric configuration is 30% higher than the drag coefficient of the full-electric configuration for all cases, due to the turboprop nacelle, which is much larger than the electric nacelles.

Furthermore, the drag coefficient increase for a nacelle is around two for the hybrid-electric configuration and around four for the full-electric configuration.

This is because the nacelles in the hybrid-electric configuration are very small, while the nacelles in the full-electric configuration are much larger.

While the full-electric configuration has a lower drag coefficient than the hybrid-electric configuration, a dedicated space is needed for the electric source on the full-electric aircraft. This may increase the overall drag of the aircraft or reduce its carrying capacity.

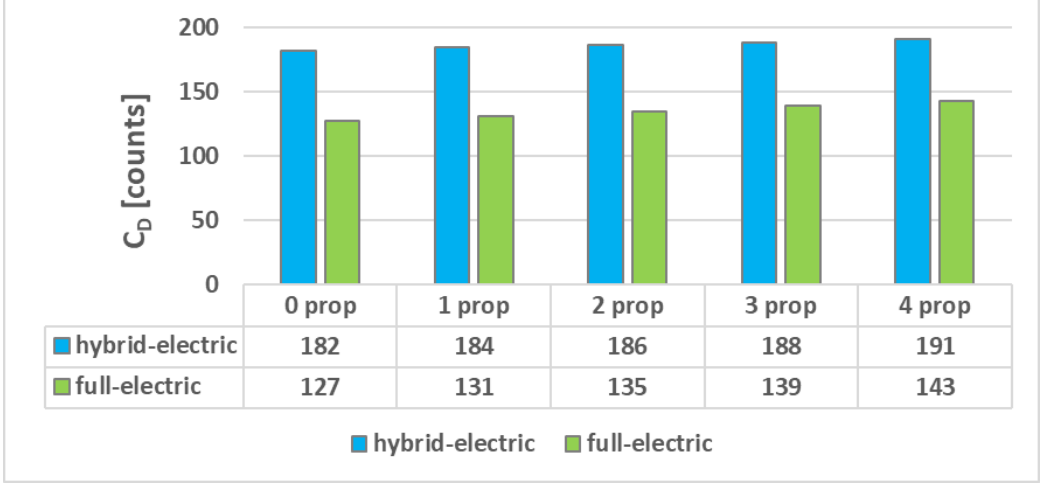

Fig. 14 – The variation of drag coefficient with the number of propellers for both hybrid-electric and full-electric configurations

3.7 Pressure coefficient distribution

For a better understanding of the propeller effect on the pressure coefficient distribution, two cases with propeller effect and without propeller effect are presented below. The presented cases are a hybrid-electric case (75p4 case) shown in Fig. 15 a) and Fig. 15c) and a full-electric case (100p4) shown in Fig. 15 b) and Fig. 15 d).

In both cases, the propeller creates a significant pressure decrease on the upper surface of the wing, which generates more lift.

Additionally, if the propellers have the same power, the smaller diameter propellers will generate a higher pressure decrease due to power concentration, as shown in Fig. 15 c) and Fig. 15 d).

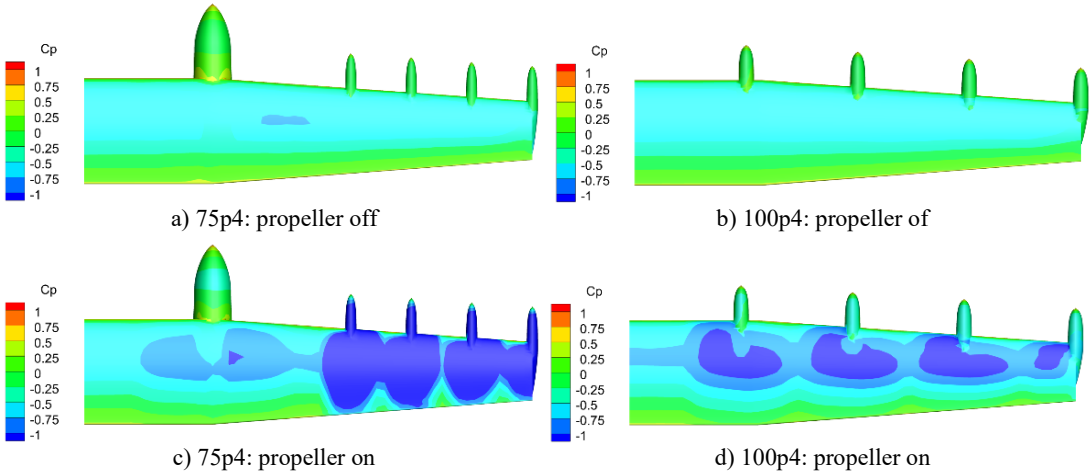

a) 75p4: propeller off b) 100p4: propeller of

c) 75p4: propeller on d) 100p4: propeller on

Fig. 15 - Pressure coefficient distribution with and without propeller effect

The pressure coefficient distribution is similar for both cases without the propeller, except for the influence of nacelles. The nacelles increase the drag force for the hybrid-electric case due to the turboprop engine nacelle.

4. CONCLUSIONS

This paper investigates the effect of propellers on lift distribution for hybrid-electric and full-electric aircraft, considering different propeller positions, numbers, powers, and spin directions. Aerodynamic analysis is used to show that wing lift and drag coefficients can be improved by carefully considering design aspects and propeller placement. Both configurations have advantages and disadvantages, so optimization is needed to find the best one.

The paper also shows that propeller position (both laterally and vertically) can significantly improve wing aerodynamic properties, even for a single propeller. Additionally, a small number of well-positioned propellers can enhance aerodynamic properties more than many propellers.

Finally, the paper shows that propeller spin direction and power have a strong effect on lift interference, causing large variations in lift distributions. The study shows that counterclockwise spin direction generates lift enhancement, and that large, concentrated power on a single wingtip propeller can significantly increase lift. The comparison of the two configurations showed that the full-electric configuration has a slightly lower drag coefficient,

but it requires an electric source to be integrated into the fuselage, which reduces cargo capacity.

In conclusion, this paper provides valuable insights into the design of hybrid-electric and full-electric aircraft, showing that the position, number, power, and spin direction of propellers can all have a significant impact on lift distribution and aerodynamic properties. The best configuration for a particular aircraft will depend on its specific requirements, but the findings from this work can be used to optimize aircraft design.

REFERENCES

[1] P. Vecchia, D. Malgieri, F. Nicolosi and A. De Marco, Numerical analysis of propeller effects on wing aerodynamic: tip mounted and distributed propulsion, in *Transport Research Procedia*, Bucharest, Romania, 2018.

[2] D. de Rosa, E. Tirado and D. Mingione, Parametric Investigation of a Distributed Propulsion System on a Regional Aircraft, *MDPI Aerospace,* vol. **9**, no. 176, 2022.

[3] Z. Cheng, Y. Yang and Y. Bo, Parameterization investigation on distributed electric propulsion aircraft aerodynamic characteristics, *Journal of Physics: Conference Series,* vol. **2459**, no. 012092, 2023.

[4] A. Stoll, J. Bevirt, M. Moore, W. Fredericks and N. Borer, Drag Reduction Through Distributed Electric Propulsion, in *Aviation Technology, Integration, and Operations Conference*, Atlanta, 2014.

[5] R. Erhard, M. Clarke and J. Alonso, A Low-Cost Aero-Propulsive Analysis of Distributed Electric Propulsion Aircraft, in *AIAA SciTech Forum*, VIRTUAL EVENT, 2021.

[6] K. Moore and A. Ning, Distributed Electric Propulsion Effects on Traditional Aircraft Through Multidisciplinary Optimization, in *AIAA SciTech Forum*, Kissimmee, 2018.

[7] E. Van, D. Alazard, P. Pastor and C. Doll, Co-design of aircraft vertical tail and control laws using distributed electric propulsion, in *IFAC Symposium on Automatic Control in Aerospace*, Cranfield, 2019.

[8] D. Vechtel and J.-P. Buch, Aspects of yaw control design of an aircraft with distributed electric propulsion, in *CEAS Aeronautical Journal*, 2022.

[9] S. Biser, M. Filipenko, M. Boll, N. Kastner, G. Atanasov, M. Hepperle, D. Keller, D. Vechtel and M. Noe, Design Space Exploration Study and Optimization of a Distributed Turbo-Electric Propulsion System for a Regional Passenger Aircraft, in *AIAA Propulsion and Energy Forum*, VIRTUAL EVENT, 2020.

[10] J. Katz and A. Plotkin, *Low-speed aerodynamics: from wing theory to panel methods*, McGraw-Hill Inc., 1991.